

University of Groningen

Voltage Deficit in Wide Bandgap Perovskite Solar Cells

Koopmans, Marten; Koster, L. Jan Anton

Published in:
Solar RRL

DOI:
[10.1002/solr.202200560](https://doi.org/10.1002/solr.202200560)

IMPORTANT NOTE: You are advised to consult the publisher's version (publisher's PDF) if you wish to cite from it. Please check the document version below.

Document Version
Publisher's PDF, also known as Version of record

Publication date:
2022

[Link to publication in University of Groningen/UMCG research database](#)

Citation for published version (APA):

Koopmans, M., & Koster, L. J. A. (2022). Voltage Deficit in Wide Bandgap Perovskite Solar Cells: The Role of Traps, Band Energies, and Effective Density of States. *Solar RRL*, 6(12), [2200560].
<https://doi.org/10.1002/solr.202200560>

Copyright

Other than for strictly personal use, it is not permitted to download or to forward/distribute the text or part of it without the consent of the author(s) and/or copyright holder(s), unless the work is under an open content license (like Creative Commons).

The publication may also be distributed here under the terms of Article 25fa of the Dutch Copyright Act, indicated by the "Taverne" license. More information can be found on the University of Groningen website: <https://www.rug.nl/library/open-access/self-archiving-pure/taverne-amendment>.

Take-down policy

If you believe that this document breaches copyright please contact us providing details, and we will remove access to the work immediately and investigate your claim.

Downloaded from the University of Groningen/UMCG research database (Pure): <http://www.rug.nl/research/portal>. For technical reasons the number of authors shown on this cover page is limited to 10 maximum.

Voltage Deficit in Wide Bandgap Perovskite Solar Cells: The Role of Traps, Band Energies, and Effective Density of States

Marten Koopmans and L. Jan Anton Koster*

Wide-bandgap (≥ 1.7 eV) perovskite solar cells (PSCs) are plagued by relatively low open-circuit voltages. This is problematic as they are key to achieving perovskite silicon tandems, which can boost the potential of silicon solar cells. Performance in PSCs is widely considered to be limited by recombination at the interface between the perovskite and the transport layer (TL). Here, a number of design rules to increase the open-circuit voltage of wide-bandgap PSCs are introduced. A numerical device model that includes a detailed description of the interfacial recombination processes is presented. The combined effects of interface traps, ions, band alignment, and transport properties are introduced to identify the critical parameters for improving the open-circuit voltage. A large number of devices are simulated by picking random combinations of parameters and are looked for trends. It is shown that interface recombination can be suppressed by reducing the minority carrier density close to the interface with the TLs. It is demonstrated that the alignment of energy levels is only part of the story; the effective densities of states are of equal importance. The results pave the way to achieving high open-circuit voltages, despite a significant density of interface defects.

1. Introduction

Perovskite solar cell (PSC) technology is maturing rapidly. Formamidinium lead iodide cells show an efficiency that is on par with silicon cells and are nearing the Shockley–Queisser limit for the open-circuit voltage.^[1] The stability of these solar cells is starting to attract more attention, as degradation mechanisms are not yet fully understood.

One of the most likely applications for PSCs is in a tandem configuration with silicon solar cells. This perovskite–silicon tandem can currently achieve 29.8% module efficiency.^[2] These tandem solar cells require perovskite subcells with a

bandgap of roughly 1.7 eV to complement the narrow bandgap cell that is most often silicon. This is problematic, however, as most of the recent efficiency improvements in PSCs have been because of a narrowing of the bandgap,^[3] which makes them less suitable for the tandem application.

Currently, good PSCs with a bandgap of around 1.7 eV typically have an open-circuit voltage (V_{oc}) of roughly 1.2 V,^[4–7] with some reaching as high as 1.28 V.^[8] While more realistic quantification exists,^[3] the difference between the radiative limit for V_{oc} and measured V_{oc} is indicative of the room for improvement. For a 1.7 eV bandgap, the radiative limit for V_{oc} is around 1.43 V, depending on the exact assumptions used to derive it.^[9] This means that in typical cells, we have a few tenths of a Volt left to improve.

Wide bandgap (≥ 1.7 eV) perovskite cells suffered from phase segregation at first, where narrow bandgap phases effectively


acted as recombination centers. It has been shown, however, that halide segregation is responsible for a smaller part of the V_{oc} loss than the electronic quality of the perovskite cells.^[6] It is, therefore, of paramount importance to understand all the factors at play at the perovskite–transport layer (TL) interface.

It is widely accepted that perovskite–TL interfaces are the main culprit of V_{oc} losses because of the presence of trap-assisted recombination.^[6,10–13] In case of a large excess of one carrier type, as is typically the case at perovskite–TL interfaces, the Shockley–Read–Hall recombination rate is determined by the minority capture rate. This means that the minority carrier density, capture coefficient, and trap density become the determinant of the interfacial recombination rate.^[14]

Surface passivation, typically by interlayers, can be employed to decrease the number of recombination centers at the perovskite–TL interface.^[11–13,15,16] Thin layers of passivating agents are deposited at the perovskite/TL interface. Even though these layers might be insulating, by keeping them very thin, they can increase rather than decrease the fill factor. Interlayers can, however, decrease recombination even without passivating recombination centers by inducing band bending to repel minority carriers from the interface.^[17]

To reduce the amount of charge carriers available for recombination at the interfaces, a few different strategies can be employed. First, a built-in voltage can contribute to extracting carriers to the right TL. Because of their n–i–p (or p–i–n)

M. Koopmans, L. J. A. Koster
Zernike Institute for Advanced Materials
University of Groningen
Groningen 9747 AG, The Netherlands
E-mail: l.j.a.koster@rug.nl

 The ORCID identification number(s) for the author(s) of this article can be found under <https://doi.org/10.1002/solr.202200560>.

© 2022 The Authors. Solar RRL published by Wiley-VCH GmbH. This is an open access article under the terms of the Creative Commons Attribution License, which permits use, distribution and reproduction in any medium, provided the original work is properly cited.

DOI: 10.1002/solr.202200560

configuration, PSCs limit surface recombination at the metal contacts by repelling minority carriers with TLs. This means that PSCs can even operate reasonably well with an electric field working against charge extraction in the perovskite.^[18] An electric field aiding charge extraction is very beneficial to cell performance, however. This electric field can be achieved by doping the TLs or by a difference in work functions between the two metal electrodes.^[18,19] The last effect can be undercut, however, by the low dielectric constant or conductivity of typical TLs, meaning most of the potential will drop over the TLs instead of the perovskite.^[20]

Additionally, an imbalance between perovskite and TL properties can play a role in repelling or attracting minority carriers to the perovskite/TL interface. Typically, TLs for PSCs are organic. Because of this, there is a large dielectric mismatch that can also cause extra recombination by the accumulation of minority carriers near the interface.^[21] While well-aligned bands between the perovskite and the TL might seem preferable, a small extraction barrier can actually increase solar cell performance as it pushes minority carriers away from the interface.^[22–24] Despite the efforts to reduce the number of interface traps, it is improbable that they can be completely prevented. It remains unclear how to optimize the electrical properties of the device stack, given that interfaces likely remain defective.

Here, we show design rules to optimize the open-circuit voltage of wide bandgap PSCs. We implement a detailed description of interfacial recombination in SIMSalabim, an open-source device modeling software. A reference device is introduced that performs like a typical wide bandgap PSC. This reference device is then used to determine the effects of interface traps, band alignment, ions, and transport properties on the open-circuit voltage.

A large number of devices are simulated with random combinations of device parameters to look for trends in the open-circuit voltage. The total recombination rate in a cell determines the open-circuit voltage. Often, a reduction of the number of interface traps is attempted to reduce recombination, but this can be experimentally challenging. We find that reducing the minority carrier density in the perovskite at the TL interface suppresses recombination in equal measure. While band alignment is often exclusively considered, we find that the effective density of states (DOS) in combination with band alignment determines the minority carrier density at the interface. We find that high

open-circuit voltages are possible despite a significant density of interfacial defects.

2. Results

To investigate wide bandgap PSCs, we will use SIMSalabim, open-source simulation software for drift–diffusion simulations.^[25] The physical model we use to represent these solar cells includes mobile ions, interfacial recombination (at TL interfaces and grain boundaries), effective DOS (N_c), energetic alignment, dielectric contrast, absorption profiles, and dopants. Mobile ions are assumed to stay in the perovskite layer except in Figures 2a and 4, where the mobile ions are allowed in the TLs at random in half of the simulations. While in a regular PSC, reflection from the back electrode is quite relevant to the absorption profile, we neglect this effect for the wide bandgap perovskites, which will be used mostly in a tandem configuration. The absorption profile is, therefore, assumed to be exponential, based on the absorption coefficient of a typical perovskite.^[26]

Figure 1a shows a schematic band diagram of the device used in our simulations, with the most important parameters used indicated in the figure at the location where they take effect. While we make the electron TL interface limiting in this work, the same results could be obtained by exchanging the electron and hole TL properties. In our simulations, we include the effect of varying dielectric constant over the device, the effective DOS in the TL (N_{c-tl}), band alignment, TL doping, TL-mobility, TL-thickness, mobile ion density, ion placement in TLs, and interfacial trap density. In line plots in this section, the generation profile is exponential starting from the left side of the device in Figure 1a. In the scatter plots, an absorption profile that is exponential starting from either electrode or a uniform absorption profile is picked at random. This is done to simulate the two edge cases for generation profiles to exclude any possible impact the detailed shape of the generation profile might have.

Because interfacial recombination is limiting to performance in most PSCs, it is imperative to model it accurately. To correctly describe the physics, we developed an advanced description of trap-assisted recombination for interface traps. We rederive the Shockley–Read–Hall recombination expression for interface traps, which can be captured from and emitted to the conduction and valence band at either side of the interface. The derivation

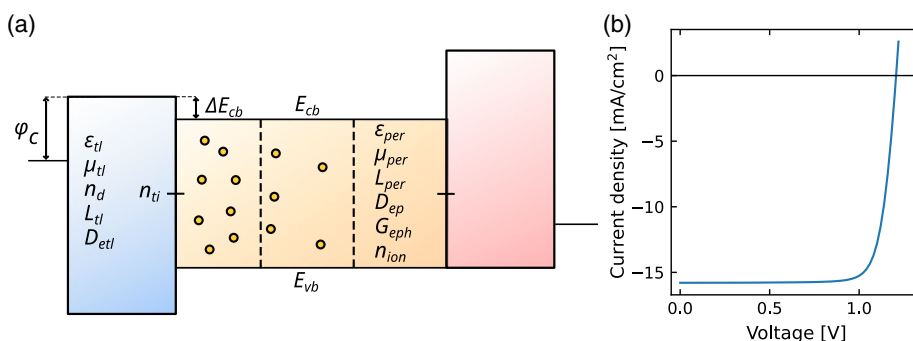


Figure 1. a) Schematic band diagram illustrating simulation parameters and where they take effect. Parameters are varied in the left transport layer (TL (Table 1)), while those in the right TL are chosen such that the left TL is limiting performance (Table S2, Supporting Information). b) Current–voltage characteristic of our reference wide bandgap perovskite solar cell (PSC). The device parameters used are in Table S1, Supporting Information.

can be found in the supporting information. Furthermore, the interface charge of traps is considered depending on the type of trap. Figure S1, Supporting Information, shows that a simpler expression for interface trapping, such as the original Shockley–Read–Hall expression, is insufficient. The large discontinuities of charge carriers' densities at the interface that are dependent on input parameters and applied voltage mean that it is not clear in advance which rates should the recombination expression if only two trapping and detrapping rates are used. Taking rates from either side of the interface into account solves this problem. The difference is illustrated in Figure S1, Supporting Information, with a band offset, but the difference can be obtained through other parameters as well.

As discussed previously, a good wide bandgap PSC currently has a V_{oc} of roughly 1.2 V and a fill factor (FF) of 0.8.^[4–7] The short-circuit current (J_{sc}) sits at roughly 15–16 mA cm⁻²,^[4–7] but is not considered for optimization in this work. As a reference point for our investigation, we introduce a device that resembles such a typical wide bandgap PSC. Device parameters are chosen such that they are close to those of real devices and yield similar performance. Using the parameters shown in Table S1, Supporting Information, we get the simulated JV curve in Figure 1b, which has a J_{sc} of 15.8 mA cm⁻², an FF of 0.81, and a V_{oc} of 1.21 V.

Figure 2a shows the reference PSC from Figure 1b where properties of the left TL, left contact, perovskite, and TL/perovskite interface were varied. Properties for the right TL and electrode are kept constant, while those on the left side are varied over a wide range indicated in Table 1. The parameters in the right TL are chosen such that they are not limiting to device performance and are shown in Table S2, Supporting Information. The results are plotted versus the trap density at the left TL/perovskite interface.

Figure 2a shows that there is a broad trend showing that fewer traps generally mean higher V_{oc} . There is, however, a wide range of possible values for V_{oc} for any trap density. This is nicely illustrated when looking at the resulting V_{oc} values at the trap density for the reference device. We see that for the reference device introduced in Figure 1b—depending on other device

Table 1. Parameters that are randomly chosen are shown on the left. A value was randomly picked between the lower and upper limits on either a linear or logarithmic scale, as indicated in the last column.

Parameter	Lower Limit	Upper Limit	Scale
Thickness TL [m]	50	50	lin
Doping TL [m ⁻³]	10 ¹⁷	10 ²³	log
Mobility TL [m ² Vs ⁻¹]	10 ⁻⁹	10 ⁻⁵	log
Perovskite/TL band offset [eV]	-0.2	0.3	lin
Contact/TL band offset [eV]	0	0.4	lin
Relative permittivity TL	3	30	lin
Effective DOS TL [m ⁻³]	10 ²²	10 ²⁸	log
Surf. trap dens. perovskite/TL int. [m ⁻²]	10 ¹²	10 ¹⁴	log
Mobile ion density [m ⁻³]	10 ¹⁶	10 ²²	log
Are ions allowed in TL (yes/no)	0	1	n.a.

parameters—the same trap density can yield a V_{oc} anywhere between 0.9 and 1.4 V.

In experiments, it is often difficult to isolate the changing of one parameter, such as interface trap density. This means that depending on other parameters that are changed along with trap density, a higher trap density could show a higher V_{oc} . Experimentally, simply reducing the number of traps regardless of other characteristics is, therefore, not an effective strategy for attaining a high V_{oc} .

Figure 2b shows that when all other parameters are kept constant, we do indeed get the expected result. Namely, starting from the trap density of the reference cell, higher trap density decreases V_{oc} and lower trap density decreases V_{oc} . In Figure 2b, three different interface trap types are considered, namely donor, acceptor, and neutral-type traps. Due to the device symmetry, donor and acceptor traps yield the same result. We will, therefore, call these charged traps. Here, a neutral trap is an unphysical type of trap that is both neutral when empty and full. This trap type is included because it can differentiate the effect of traps contributing as recombination centers and traps contributing to space charge.

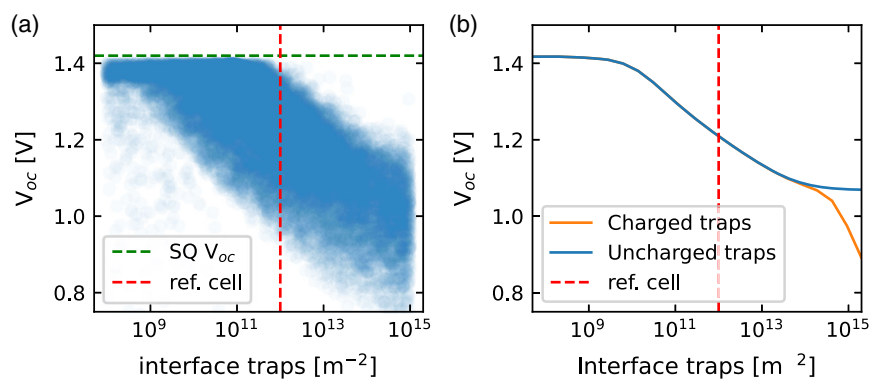


Figure 2. a) We vary relevant solar cell properties from our reference cell (red dashed line), except for those in the right TL and right contact. The parameter ranges are indicated in Table 1. b) The dependence of V_{oc} on interface trap density for charged traps and uncharged traps. Charged traps are traps that are either negatively charged when filled with an electron (acceptor type) or positively charged when empty, or not filled with an electron (donor type). Uncharged traps are a limit of low trap density but high capture coefficients, which means that these traps do not contribute to space charge, but do act as recombination centers.

In Shockley–Read–Hall recombination, the trap density and capture coefficient only appear as a product, which is a recombination velocity as it has unit m s^{-1} .^[14] If the charge of the traps does not play a role, the recombination velocity can uniquely determine recombination and therefore V_{oc} in our simulations. Since the simulations are performed in steady state, we can then disentangle the effect from recombination and charge of the trap.

We see in Figure 2b that at low trap densities, the charge of the trap does not play a role as the neutral type trap gives the same V_{oc} as the charged traps. At trap densities above 10^{14} m^{-2} , however, we see that charged traps have significantly lower V_{oc} than uncharged traps. This shows that interface traps can be considered just as recombination centers without charge for low to medium interface trap densities. The leveling off of the V_{oc} at high trap density for neutral traps can be explained by minority carrier depletion at the interface; if there are a negligible number of minority carriers at the interface at V_{oc} , recombination does not increase further upon the addition of more traps. This teaches us that the charge of interface traps is unlikely to be relevant for cells that have a V_{oc} of 1.2 V, the state of the art.

We continue our investigation by looking at the effect of the effective DOS (N_c) on V_{oc} . The N_c is determined by an integral over the product of the Fermi–Dirac distribution and the DOS of the material in question. For typical inorganic materials, the DOS is parabolic, which means that this integral returns a constant, the N_c times a Boltzmann factor.^[27]

This same simplification does not hold however for organic materials, which typically have a Gaussian DOS.^[28] The Gaussian DOS causes an increase in N_c , increasing it above the total integral of the Gaussian DOS when the (quasi-)Fermi level gets close to the lowest unoccupied molecular orbital (LUMO) level. This is the case in a good solar cell near V_{oc} .

In Figure 3a, it seems very intuitive that the organic layer should have a higher charge carrier density. In our simulations, this effect is captured by the N_c , which is orders of magnitude higher for organic materials. To keep the charge carriers from accumulating in the organic layer, the LUMO level can be increased to compensate for the increased N_{c-tl} .

Figure 2 shows that despite a significant number of traps, achieving a good V_{oc} is possible. To investigate further what improvements can be made without reducing the number of traps, we will now select all solar cells from the dataset with trap densities of $3 \times 10^{11} \text{ m}^{-2}$ and upwards. This means that the trap density is close to that of the reference device introduced in Figure 1 or above that. Figure 3 implies that to counteract higher N_c in the TL than the perovskite, the conduction band of the TL should be increased to counteract charge carrier accumulation. To test this premise, we take the same simulations as in Figure 2, which include: mobile ion density, TL mobility, generation profile, TL/perovskite band offset, relative permittivity of the TL, TL thickness, TL doping density, electrode work function, interface trap density, and N_c of the TL. These simulations are then plotted against different parameters to show trends in V_{oc} .

The result is shown in Figure 4 for the subset of devices with a trap density above $3 \times 10^{11} \text{ m}^{-2}$ as mentioned earlier. The points show all simulations, plotted against different variables in different sub-figures. In Figure 4a,b, the data are plotted against the N_{c-tl} in the TL and the conduction band offset. While a trend is visible, neither band alignment nor the effective DOS provides a

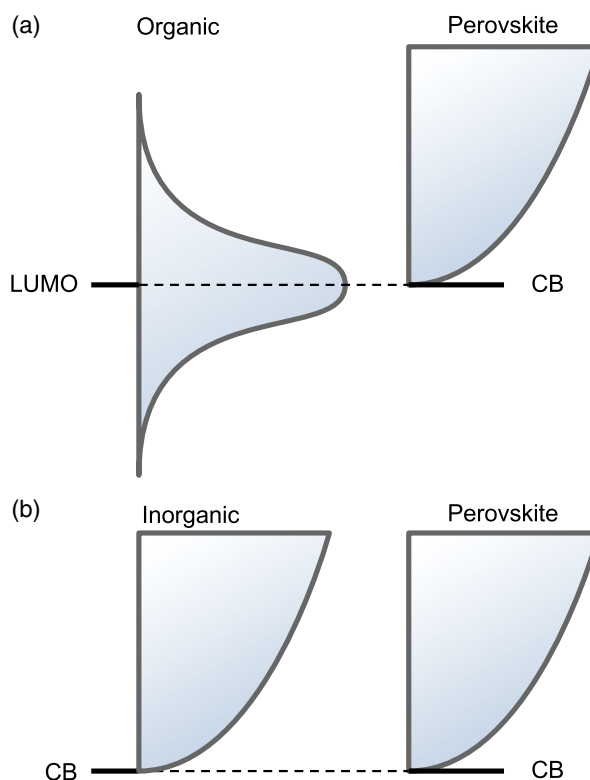


Figure 3. This figure shows schematically the difference between perfectly aligned bands for: a) organic-TL/perovskite junctions, where the lowest unoccupied molecular orbital (LUMO) of the organic layer defines the center of a Gaussian DOS and b) inorganic-TL/perovskite junctions, where both the inorganic-TL and the perovskite have a parabolic band defined by the minimum of the parabola.

clear relation with V_{oc} . In Figure 4c, the data are plotted against the parameter

$$\omega_{int} = C_{min} N_{ti} \frac{N_{c-tl}}{N_{c-per}} \exp\left(\frac{\Delta E_c}{k_B T}\right) \quad (1)$$

where C_{min} is the minority carrier capture coefficient, N_{ti} is the interfacial trap density, and $N_{c-tl/per}$ are the effective DOS of the TL and perovskite. This parameter approximates recombination at the interface by just the rate of minority carrier trapping $C_{min} n_{min} N_{ti}$, where n_{min} is the minority carrier density. As a gradient in N_c or band energy causes a step in the electrostatic potential at the interface, the minority carrier density changes accordingly. Typical TLs are blocking for minority carriers, however, so increased minority carrier density in the TL is not the cause for increased recombination.

Instead, the increased carrier density over the TL causes a larger potential drop in the TL, decreasing the potential drop over the perovskite layer. This large potential drop over the TL means there is a less potential drop over the perovskite to keep minority carriers from the interface. This increase of minority carrier density near the interface increases recombination and reduces V_{oc} . With a given N_c offset between TL and active layer, this means that band alignment can be used to engineer a low carrier

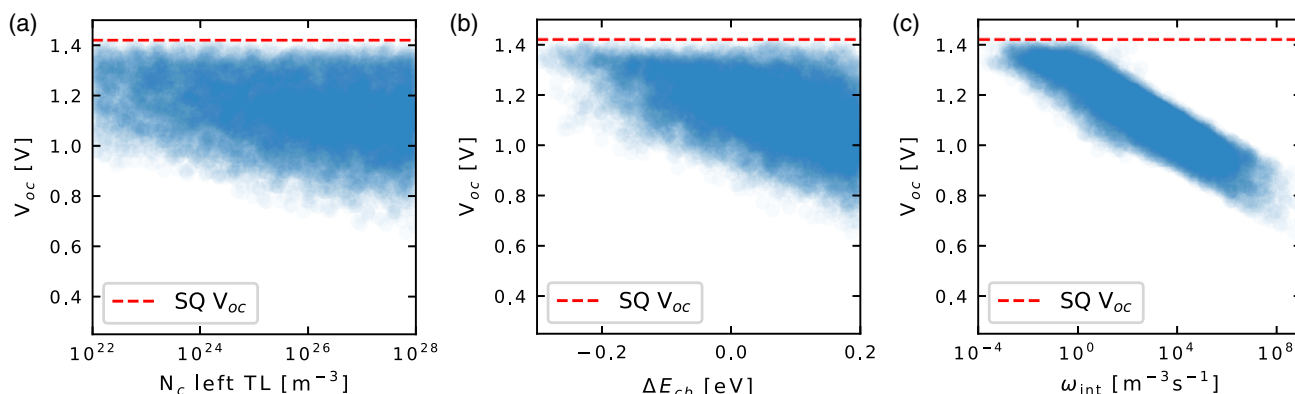


Figure 4. The dots show all simulations ran using parameters randomly drawn from the ranges indicated in Table 1. The Shockley–Queiser V_{oc} is plotted as a red dotted line. a) All simulations plotted against the density of states (DOS) in the TL. b) All simulations plotted against the difference between the perovskite and the TL conduction band. c) All simulations plotted against parameter ω_{int} .

density near the interface, reducing recombination. While a high N_c , typical of organic TLs, can still result in a high V_{oc} , this can happen if and only if the high N_c is compensated with a TL conduction band that lies higher than the perovskite conduction band.

Experimental verification of the results in Figure 4 and Equation (1) is hindered by the fact that values of the effective DOS are rarely reported. To verify our results, we study the effect of the disorder in the TL on V_{oc} . Less disorder implies a smaller effective DOS, and thus an improved V_{oc} . As the disorder is typically hard to reduce from an already decent TL, this effect is relatively minor. Nonetheless, it will impact the N_{c-tl} , allowing us to verify our results. While the exact N_{c-tl} is unknown, we can calculate the decrease in N_{c-tl} that would result from a decrease in disorder in an organic Gaussian DOS, assuming that only disorder changes between two solar cells in the parameter ω_{int} from Equation (1). Assuming the same trend of V_{oc} versus ω_{int} as in Figure 4c, the change in N_{c-tl} resulting from a change in disorder can be converted to a change in V_{oc} . Using this procedure to predict the V_{oc} increase from a reduction in TL disorder as

reported in the literature,^[29–31] we find that the agreement is satisfactory (See Table S3, Supporting Information). For details on this procedure, we refer to the supporting information.

Figure 5 shows the effect of changing the conduction band level for different N_c in the reference device introduced in Figure 1b. In Figure 5a, shows that to attain maximum V_{oc} , the conduction band or LUMO of the TL should be equal to or higher than (depending on the N_c) the conduction band of the perovskite, which is set at 3.3 eV in the simulations. When the N_c of the perovskite equals that of the TL, optimal efficiency is obtained by aligning the TL and perovskite conduction bands. When the N_c of the TL increases, however, both the FF and V_{oc} increase when the conduction band of the TL is raised. This yields a maximum power point (MPP) peak at a conduction band energy in the TL that is higher. This difference, ΔE_{cb} , is roughly 0.1 eV, for an N_c in the TL of 10^{27} m^{-3} , realistic for an organic layer with aligned bands. This shows that a higher N_c can be effectively counteracted by de-aligning the bands according to the parameter ω_{int} from Equation (1), to reduce the carrier density in the TL.

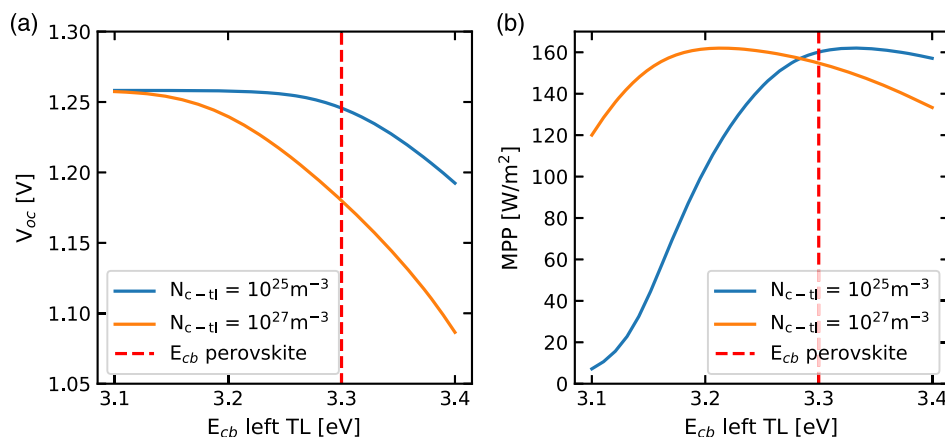


Figure 5. The effect of the conduction band energy (E_{cb}) on: a) V_{oc} and b) the maximum power point (MPP) of our reference solar cell. N_{c-tl} is varied from being equal to that of the perovskite layer at 10^{25} m^{-3} , to higher by a factor of 100. The conduction band energy of the perovskite is shown as a reference.

3. Discussion

Suppose we start from a medium bandgap device with optimal TLs in terms of band alignment and N_c and then increase the bandgap. This means that we will get alignment problems at one or both of the TL/perovskite interfaces that forces an increased carrier density in the TL, decreasing V_{oc} . To reduce interfacial recombination—and to enhance V_{oc} —one can focus on reducing the number of interface traps, their capture coefficients, or the minority carrier density near the TLs.

Optimal band alignment in PSCs can be counterintuitive. While it is known that we need different TLs for wide bandgap devices,^[32] it is mostly suggested that aligned bands are best. This depends, however, on the effective DOS offset between perovskite and TL. Perfect energetic alignment of bands between perovskite and TL can yield worse performance than a TL that shows a small extraction barrier.^[23] This effect is strongest for organic TLs with a high DOS per unit volume and a Gaussian DOS.^[28]

We show that the DOS offset between the perovskite layer and TL should also be considered when determining optimal band alignment. Since typical organic TLs have a higher N_c than typical perovskite layers, it can be seen in Figure 4 that an extraction barrier leads to higher V_{oc} at the same trap density. Interestingly, a realistic N_c of 10^{27} to 10^{28} m^{-3} coincides with a V_{oc} of 1.2 V or lower in our simulations.

Experimentally, it has been observed that lower disorder in the TL leads to a higher V_{oc} .^[29–31] This is often attributed to better transport, but we show that the effect is more subtle than that; higher disorder means a wider Gaussian DOS, leading to more states closer to the Fermi level yielding a higher N_c in the TL. This results in a reduced potential drop over the perovskite, leading to higher minority carrier density near the perovskite/TL interface and therefore a lower V_{oc} .

We show that the problem of reduced V_{oc} can be solved by reducing disorder, leading to a lower N_c , by increasing the band offset between ΔE_c , or reducing the density of traps at the interface as shown by Equation (1). It should be highlighted that these effects are interchangeable in terms of V_{oc} , so the method that experimentally is the most feasible can be chosen for specific device configurations.

This agrees with what we illustrate in Figures 3 and 5; More specifically, the width of this Gaussian is typically around 0.1 eV and reducing it from 0.136 to 0.090 eV increased V_{oc} by 0.09 V experimentally,^[29] which is highly significant.

The dielectric constant might be expected to have a large influence on V_{oc} via a reduction of the built-in potential^[33] or by trapping carriers near the interface.^[21] We find, however, that while the dielectric mismatch can have a large effect on the FF via lowering of the built-in potential, its effect on V_{oc} is rather limited.

4. Conclusions

In conclusion, we introduce design rules for achieving optimal V_{oc} in PSCs. To this end, we provide a device model including a detailed description of interfacial recombination and use this to simulate a typical wide bandgap PSC. We then simulate a large set of solar cells including the effects of ions, transport properties, band alignment, and traps. The total recombination rate in a

device determines the open-circuit voltage, but is affected by different device parameters.

We introduce a parameter that combines the effect of interfacial trapping, N_c offset, and band alignment. The obvious strategy to reduce recombination and increase V_{oc} is to reduce the number of interfacial traps, which is experimentally challenging. We show that recombination can be suppressed by reducing the minority carrier density near the interface by tuning the band alignment and N_c offset at the interface. This means that band alignment is only half of the story and for achieving high V_{oc} , the N_c is of equal importance. Together, our results show that V_{oc} can get close to the Shockley-Queisser limit despite a significant number of interface traps.

5. Experimental Section

In the recent past, we adapted our device model to make it more suitable for simulations on PSCs.^[10,34] The model solves a discretized form of the 1D classic drift-diffusion equations

$$J_n = -qn\mu_n \frac{\partial V}{\partial x} + qD_n \frac{\partial n}{\partial x} \quad (2)$$

for electrons and

$$J_p = -qp\mu_p \frac{\partial V}{\partial x} + qD_p \frac{\partial p}{\partial x} \quad (3)$$

for holes, respectively, where J_n and J_p are the electron and hole current densities, q is the unit charge, n and p are the electron and hole densities, μ_n and μ_p are the electron and hole mobilities, V is the electrostatic potential, and D_n and D_p are the electron and hole diffusion constants following from the Einstein relations.^[35] The unknowns in these equations are the electrostatic potential, and the electron and hole densities. The electrostatic potential can be solved from Poisson's equation

$$\frac{\partial^2}{\partial x^2} V(x) = -\frac{q}{\epsilon(x)} (p(x) - n(x) + N_D^+(x) - N_A^-(x) + \sigma_{tr}^{bulk} + \sigma_{tr}^{int} + I^+ - I^-) \quad (4)$$

where ϵ is the permittivity, N_D^+ and N_A^- are the ionized p-type and n-type doping density, and I^+ and I^- are the positive and negative, possibly mobile, ion densities, and σ_{tr}^{bulk} and σ_{tr}^{int} are the bulk and interface trap charge density. A Schottky contact at the contacts is assumed at the boundaries of the simulations volume, resulting in a boundary condition for the Poisson equation of the form

$$q(V(L) - V(0)) = W_c - W_a - V_{app} \quad (5)$$

where $V(L)$ and $V(0)$ are the electrostatic potentials at the cathode and anode, respectively, W_c and W_a are the work functions of the cathode and anode, and V_{app} is the applied voltage between the cathode and anode.

Charge carrier generation, recombination, and extraction are governed by the continuity equations

$$G = \frac{\partial n}{\partial t} - \frac{1}{q} \frac{\partial J_n}{\partial x} \quad (6)$$

$$G = \frac{\partial p}{\partial t} + \frac{1}{q} \frac{\partial J_p}{\partial x} \quad (7)$$

where G is the net generation rate, or recombination if G is negative, per unit time. What is left is to define expressions for generation and recombination. Two different recombination mechanisms are included. The band-to-band recombination rate is determined by

$$R_b = k_b(np - n_i^2) \quad (8)$$

where k_b is the band-to-band recombination constant, and n_i is the intrinsic carrier density. Trap-assisted recombination, or Shockley–Read–Hall recombination is governed by

$$R_{SRH} = \frac{C_n C_p (N_{\text{trap}} + P_{\text{trap}})}{C_n (n + n_o) + C_p (p + p_o)} (np - n_i^2) \quad (9)$$

where R_{SRH} is the Shockley–Read–Hall recombination rate, C_n and C_p are the electron and hole capture coefficients of traps, N_{trap} and P_{trap} are the electron and hole trap densities, and n_o and p_o are defined as

$$n_o = N_c \exp\left(-\frac{E_c - E_{\text{trap}}}{k_B T}\right) \quad (10)$$

$$p_o = N_v \exp\left(\frac{E_v - E_{\text{trap}}}{k_B T}\right) \quad (11)$$

where N_c is the DOS, E_c and E_v are the conduction and valence band energies, E_{trap} is the trap energy, k_B is Boltzmann's constant, and T is the temperature. In our device model, traps can be present at the perovskite–TL interface, at the grain boundaries of the perovskite, and in the bulk. For interface trapping, the rate equations can be found in the supporting information.

The generation of carriers is determined by light absorption in the perovskite, which varied between uniform, exponential from the n-side of the device and exponential from the p-side of the device. Because of the low exciton binding energy in perovskite light absorption is assumed to always result in free carriers.^[36]

In Figure 4, a large range of parameters is scanned to obtain the different data points. In Table 1, these parameter ranges are shown.

Supporting Information

Supporting Information is available from the Wiley Online Library or from the author.

Acknowledgements

The authors would like to thank the Center for Information Technology of the University of Groningen for their support and for providing access to the Peregrine high performance computing cluster. This work is part of the research program of the Foundation for Fundamental Research on Matter (FOM), which is part of the Netherlands Organization for Scientific Research (NWO). This is a publication by the FOM Focus Group “Next Generation Organic Photovoltaics,” participating in the Dutch Institute for Fundamental Energy Research (DIFFER).

Conflict of Interest

The authors declare no conflict of interest.

Data Availability Statement

Research data are not shared

Keywords

drift–diffusion modeling, perovskite solar cells, photovoltaics, recombination

Received: June 22, 2022
Revised: August 26, 2022
Published online: October 28, 2022

- [1] Z. Liu, L. Kriickemeier, B. Krogmeier, B. Klingebiel, J. A. Marquez, S. Levchenko, S. Oz, S. Mathur, U. Rau, T. Unold, T. Kirchartz, *ACS Energy Lett.* **2019**, *4*, 110.
- [2] Best Research-Cell Efficiency Chart, <https://www.nrel.gov/pv/cell-efficiency.html> (accessed: December 2021).
- [3] L. Kriickemeier, U. Rau, M. Stolterfoht, T. Kirchartz, *Adv. Mater.* **2020**, *10*, 1902573.
- [4] S. Kavadiya, A. Onno, C. C. Boyd, X. Wang, A. Cetta, M. D. McGehee, Z. C. Holman, *Sol. RRL* **2021**, *5*, 2100107.
- [5] L. Gil-Escrig, C. Dreessen, F. Palazon, Z. Hawash, E. Moons, S. Albrecht, M. Sessolo, H. J. Bolink, *ACS Energy Lett.* **2021**, *6*, PMID: 34568574, 827.
- [6] S. Mahesh, J. M. Ball, R. D. J. Oliver, D. P. McMeekin, P. K. Nayak, M. B. Johnston, H. J. Snaith, *Energy Environ. Sci.* **2020**, *13*, 258.
- [7] X. Liu, Z. Wu, X. Fu, L. Tang, J. Li, J. Gong, X. Xiao, *Nano Energy* **2021**, *86*, 106114.
- [8] Z. Xu, X. Liu, S. Fu, J. Wang, J. Zhang, L. Huang, Z. Hu, Y. Zhu, *Appl. Phys. Lett.* **2021**, *119*, 212101.
- [9] W. Shockley, H. J. Queisser, *J. Appl. Phys.* **1961**, *32*, 510519.
- [10] T. S. Sherkar, C. Momblona, L. Gil-Escrig, H. J. Bolink, L. J. A. Koster, *Adv. Mater.* **2017**, *7*, 1602432.
- [11] L. Kriickemeier, B. Krogmeier, Z. Liu, U. Rau, T. Kirchartz, *Adv. Mater.* **2021**, *11*, 2003489.
- [12] M. Stolterfoht, C. M. Wolff, J. A. Marquez, S. Zhang, C. J. Hages, D. Rothhardt, S. Albrecht, P. L. Burn, P. Meredith, T. Unold, D. Neher, *Nat. Energy* **2018**, *3*, 847.
- [13] Q. Jiang, Y. Zhao, X. Zhang, X. Yang, Y. Chen, Z. Chu, Q. Ye, X. Li, Z. Yin, J. You, *Nat. Photonics* **2019**, *13*, 460.
- [14] W. Shockley, W. T. Read, *Phys. Rev.* **1952**, *87*, 835.
- [15] M. A. Mahmud, T. Duong, Y. Yin, H. T. Pham, D. Walter, J. Peng, Y. Wu, L. Li, H. Shen, N. Wu, N. Mozaffari, G. Andersson, K. R. Catchpole, K. J. Weber, T. P. White, *Adv. Funct. Mater.* **2020**, *30*, 1907962.
- [16] M. Hadadian, J.-P. Correa-Baena, E. K. Goharshadi, A. Ummadisingu, J.-Y. Seo, J. Luo, S. Gholipour, S. M. Zakeeruddin, M. Saliba, A. Abate, M. Gratzel, A. Hagfeldt, *Adv. Mater.* **2016**, *28*, 8681.
- [17] H. Wang, Y. Song, S. Dang, N. Jiang, J. Feng, W. Tian, Q. Dong, *Sol. RRL* **2020**, *4*, 1900468.
- [18] U. Wiirfel, A. Cuevas, P. Wiirfel, *IEEE J. Photovoltaics* **2015**, *5*, 461.
- [19] J. Diekmann, P. Caprioglio, M. H. Futscher, V. M. Le Corre, S. Reichert, F. Jaiser, M. Arvind, L. P. Toro, E. Gutierrez-Partida, F. Pena-Camargo, C. Deibel, B. Ehrler, T. Unold, T. Kirchartz, D. Neher, M. Stolterfoht, *Sol. RRL* **2021**, *5*, 2100219.
- [20] N. E. Courtier, J. M. Cave, J. M. Foster, A. B. Walker, G. Richardson, *Energy Environ. Sci.* **2019**, *12*, 396.
- [21] T. S. Sherkar, L. J. A. Koster, *ACS Appl. Mater. Interfaces* **2015**, *7*, PMID: 25989847, 11881.
- [22] J. Dong, J. Shi, D. Li, Y. Luo, Q. Meng, *Appl. Phys. Lett.* **2015**, *107*, 073507.
- [23] C. Ding, Y. Zhang, F. Liu, Y. Kitabatake, S. Hayase, T. Toyoda, K. Yoshino, T. Minemoto, K. Katayama, Q. Shen, *Nano Energy* **2018**, *53*, 17.
- [24] T. Yokoyama, Y. Nishitani, Y. Miyamoto, S. Kusumoto, R. Uchida, T. Matsui, K. Kawano, T. Sekiguchi, Y. Kaneko, *ACS Appl. Mater. Interfaces* **2020**, *12*, PMID: 32427458, 27131.
- [25] M. Koopmans, V. M. L. Corre, L. J. A. Koster, *J. Open Source Software* **2022**, *7*, 3727.

- [26] S. De Wolf, J. Holovsky, S.-J. Moon, P. Loper, B. Niesen, M. Ledinsky, F.-J. Haug, J.-H. Yum, C. Ballif, *J. Phys. Chem. Lett.* **2014**, *5*, PMID: 26270984, 1035.
- [27] C. Kittel, *Introduction to Solid State Physics*, 8th ed., Wiley, New York, NY **2004**.
- [28] H. Bassler, D. Kroh, F. Schauer, V. NadaZdy, A. Kohler, *Adv. Funct. Mater.* **2021**, *31*, 2007738.
- [29] Y. Shao, Y. Yuan, J. Huang, *Nat. Energy* **2016**, *1*, 15001.
- [30] Y. Jiang, J. Wang, H. Zai, D. Ni, J. Wang, P. Xue, N. Li, B. Jia, H. Lu, Y. Zhang, F. Wang, Z. Guo, Z. Bi, H. Xie, Q. Wang, W. Ma, Y. Tu, H. Zhou, X. Zhan, *J. Am. Chem. Soc.* **2022**, *144*, 5400.
- [31] G. Xu, R. Xue, S. J. Stuard, H. Ade, C. Zhang, J. Yao, Y. Li, Y. Li, *Adv. Mater.* **2021**, *33*, 2006753.
- [32] Y. Lin, B. Chen, F. Zhao, X. Zheng, Y. Deng, Y. Shao, Y. Fang, Y. Bai, C. Wang, J. Huang, *Adv. Mater.* **2017**, *29*, 1700607.
- [33] J.-Y. Huang, Y.-W. Yang, W.-H. Hsu, E.-W. Chang, M.-H. Chen, Y.-R. Wu, *Sci. Rep.* **2022**, *12*, 7927.
- [34] T. S. Sherkar, C. Momblona, L. Gil-Escrig, J. Avila, M. Sessolo, H. J. Bolink, L. J. A. Koster, *ACS Energy Lett.* **2017**, *2*, 1214.
- [35] S. Selberherr, *Analysis and Simulation of Semiconductor Devices*, Springer, Vienna **1984**.
- [36] A. Miyata, A. Mitioglu, P. Plochocka, O. Portugall, J. T. W. Wang, S. D. Stranks, H. J. Snaith, R. J. Nicholas, *Nat. Phys.* **2015**, *11*, 582.